Regenerability of a Ni catalyst in the in-line catalytic steam reforming of biomass pyrolysis volatiles

Aitor Arregi, Gartzen Lopez, Maider Amutio, Itsaso Barbarias, Laura Santamaria, Javier Bilbao and Martin Olazar

Department of Chemical Engineering, University of the Basque Country UPV/EHU, P.O. Box 644 - E48080 Bilbao (Spain). gartzen.lopez@ehu.eus

Abstract

A study has been carried out of the regenerability of a commercial Ni catalyst used in the steam reforming of volatiles from biomass pyrolysis, determining the evolution of the reaction indices in successive reaction-regeneration cycles. The causes of catalyst deactivation (coke deposition and Ni sintering) have been ascertain characterizing the deactivated and regenerated catalysts by TPO, TEM, TPR and XRD. Catalyst activity is not fully recovered by coke combustion in the first cycles due to the irreversible deactivation by Ni sintering, but the catalyst reaches a pseudo-stable state beyond the fourth cycle, reproducing its behaviour in subsequent cycles.

Keywords: biomass; pyrolysis; reforming; hydrogen; deactivation; regeneration

1. Introduction

H_2 production from renewable sources is a pressing need for meeting the growing demand for ammonia and methanol production in the chemical industry and oil refining, as well as for its future use as a clean energy carrier [1]. Accordingly, the processes of H_2 production from lignocellulosic biomass have received great attention in order to partially replace the current processes based on non-renewable sources, such as natural gas, oil derivates and coal [2].

Biomass pyrolysis is one of the most promising thermochemical routes for biomass valorization, given that all pyrolysis products (bio-oil, gases and char) may be converted into fuels and chemicals [3]. Recently, the production of H_2 from biomass has been proposed through a two in-line reactor system, the former for biomass pyrolysis and the

latter for the reforming of nascent volatiles [4-8]. This strategy is as an alternative to other biomass valorization routes, such as steam gasification [9-12] and bio-oil reforming [13-18], and avoids the problems related to tar formation and bio-oil handling, respectively [19]. Previous studies by the research group reported the good performance of the conical spouted bed reactor (CSBR)-fluidized bed reactor (FBR) system for pyrolysis and in-line reforming of the pyrolysis volatiles derived from biomass [5,20,21], plastics [22-25] and biomass/plastic mixtures [26].

Although noble metals, such as Pt, Pd and Rh, have a higher activity for reforming processes [27-30], Ni-based catalysts are the most common ones for the reforming of oxygenated compounds [31-33] and hydrocarbons [34-36], whose use is motivated mainly by its low cost and availability. Nevertheless, the deactivation of the catalyst due to coking is more severe on Ni-based catalysts than on noble metal ones [37]. Ochoa et al. [38] studied the deactivation of a Ni commercial catalyst in the pyrolysis and in-line catalytic steam reforming of high density polyethylene (HDPE) and reported that Ni sintering and coke deposition are the main deactivating causes. Furthermore, deactivation is faster in the reforming of biomass pyrolysis volatiles than in the reforming of plastic pyrolysis volatiles because phenolic oxygenates produce amorphous coke, which encapsulates Ni active sites [37,39]. Consequently, the main challenge in the reforming of biomass pyrolysis volatiles should focus the attenuation of Ni catalyst deactivation and its regeneration. Although studies of coke deposition and its characterization have been approached in the pyrolysis and in-line catalytic steam reforming of biomass [40-42] and plastics [36,43], those involving catalyst regeneration are rather scarce and deal exclusively with the reforming of hydrocarbons, such as methane [44,45], and pure oxygenate compounds, such as ethanol [46-50], dimethyl ether [51,52] or glycerol [53,54]. Li et al. [55] studied the steam reforming of biomass tar on a Ni-Fe/Mg/Al catalyst, which shows better regenerability than that of Ni-Fe/α-Al_2O_3. Montero et al. [49] regenerated a Ni/La_2O_3-αAl_2O_3 by coke combustion at 550 ºC for 2 h and performed successive ethanol reforming-regeneration cycles subsequent to a catalyst equilibration step consisting in a slight deactivation of the catalyst by partial Ni sintering.

Based on this background, this paper aims at regenerating a commercial Ni reforming catalyst by coke combustion with air in order to ascertain its behaviour in successive reforming-regeneration cycles. Thus, the evolution of conversion, product yields and

gas composition under reforming-regeneration cycles has been monitored. Moreover, in order to explain the results obtained, the deactivated and regenerated catalysts have been characterized by different techniques.

2. Experimental

2.1. Biomass and catalyst properties

The biomass used is forest pine wood waste *(pinus insignis)*, whose main properties are summarized in Table 1. The ultimate and proximate analyses have been determined in a *LECO CHNS-932* elemental analyzer and *TGA Q5000IR* thermogravimetric analyzer, respectively, and the higher heating value (HHV) has been measured in a *Parr 1356* isoperibolic bomb calorimeter. The biomass has been crushed, ground and sieved to a particle size between 1 and 2 mm. This particle size allows continuously feeding low flow rates and providing the heat transfer required for the pyrolysis step.

Table 1. Properties of the pine wood sawdust.

Ultimate analysis (wt %)	
Carbon	49.33
Hydrogen	6.06
Nitrogen	0.04
Oxygen	44.57
Proximate analysis (wt %)	
Volatile matter	73.4
Fixed carbon	16.7
Ash	0.5
Moisture	9.4
HHV (MJ kg^{-1})	19.8

A Ni reforming catalyst (NiO content 14 wt %), commercialized for CH_4 reforming has been used. The catalyst (G90LDP, provided by *Süd Chemie*) has been crushed and sieved to a particle size in the 0.4-0.8 mm range in order to obtain a suitable fluidization regime. The superficial properties of the catalyst (determined by N_2 adsorption-desorption in a *Micromeritics ASAP 2012* equipment) are as follows: BET surface area, 19 $m^2\ g^{-1}$; pore volume, 0.04 $cm^3\ g^{-1}$, and; average pore diameter, 122 Å.

The coke content deposited on the deactivated catalyst has been determined at the end of each reaction step by temperature programmed oxidation (TPO) in a thermobalance *TA Instruments TGA Q5000* connected to a *Balzers Instruments Thermostar* mass spectrometer in order to measure the concentration of CO_2 at the reactor outlet. In addition, the nature of the coke deposited has been analyzed by transmission electron microscopy (TEM) images (*Philips CM200*).

The catalyst regenerated at the end of each cycle has been analyzed by X-ray diffraction (XRD) technique in a *Philips X'PERT PRO* diffractometer. The average Ni^0 particle size has been determined by applying the Debye-Scherrer approach at $2\theta = 52$ º, corresponding to Ni^0 (2 0 0) plane. Moreover, the different reducible metallic species of the fresh and regenerated catalysts have been determined by temperature programmed reduction (TPR) in a *Micromeritics AutoChem 2920*.

2.2. Reaction equipment

The reaction system has been described in previous studies [5,20] and consists of the following elements: a conical spouted bed reactor (CSBR) for the steam pyrolysis and a fluidized bed reactor (FBR) for the reforming step. Both reactors are located inside a forced convection oven in order to maintain the box temperature at 300 ºC and avoid the condensation of heavy compounds in the pipes. The main dimensions of the CSBR are as follows: height of the conical section, 73 mm, diameter of the cylindrical section, 60.3 mm, angle of the conical section, 30 º, diameter of the bed bottom, 12.5 mm, and diameter of the gas inlet, 7.6 mm. Moreover, a gas preheater was located below the CSBR, which consists of a stainless steel cylindrical shell, filled with stainless steel pipes in order to increase the surface area for heat transfer and heat the gases to the reaction temperature. The gas preheater and CSBR are located inside an oven consisting of a stainless steel shell with the walls filled with ceramic fibre. The oven is 52 cm long, with 1250 W power, and provides the heat required to reach the reaction temperature and preheat the gaseous stream to the reaction temperature. The char formed has been continuously removed by means of a lateral outlet pipe to avoid its accumulation in the bed. This separation has been achieved based on the different trajectories described by char particles in the CSBR [56,57].

The FBR is a cylindrical steel reactor, with a length of 440 mm and an internal diameter of 38.1 mm. It is located inside an oven consisting of a stainless steel shell with the walls filled with ceramic fibre, which is 305 mm long and 550 W power. This oven provides the heat required to maintain the reaction temperature, which is controlled by means of a thermocouple placed inside the catalyst bed.

The pilot plant is provided with systems for feeding solid, water and gas. The system for feeding the biomass into the pyrolysis reactor consists of a dosage cylinder with 20 mm in internal diameter, provided with 40 cm stroke piston, which pushes the solid towards the top of the feeding system. By ascending the piston, the biomass falls into the reactor through a tube, which is cooled with tap water. A very small flow rate of an inert gas (N_2) is fed to ease the solid flow into the reactor and avoid the condensation of pyrolysis volatiles and steam in the dispenser. Moreover, the water required for generating the steam for the reforming step and for the fluidization of both reactors (spouted and fluidized beds) has been driven by a high pressure pump *Gilson 307*. Moreover, the product separation system consists of a gas-solid separation system provided with a cyclone and a filter, and a gas-liquid separation system consisting of a condenser and a coalescence filter.

The on-line analysis of the volatiles from the reforming step has been carried out by means of a GC *Agilent 6890* provided with a HP-Pona column and a flame ionization detector (FID). The sample has been injected into the gas chromatograph through a line thermostated at 280 ºC. Furthermore, the non-condensable gases have been analyzed on-line in a micro GC *Varian 4900*, once the water and non-reacted liquid products have been removed by condensation.

2.3. Experimental conditions

The pyrolysis step has been carried out at 500 ºC, which is the suitable temperature in order to maximize bio-oil production [58]. The biomass and water have been fed into the CSBR in a continuous regime by feeding 0.75 g min^{-1} and 3 mL min^{-1}, respectively, which corresponds to a steam/biomass ratio (S/B) of 4. In order to guarantee a vigorous movement of the bed and avoid its defluidization, 50 g of sand have been used with a particle diameter in the 0.30-0.35 mm range. Under these pyrolysis conditions, 75.3 wt % of bio-oil, 7.3 wt % of gases and 17.3 wt % of char are produced in the CSBR [5],

143 with their detailed composition being shown in Table 2. The char has been recovered
144 from the CSBR by a lateral outlet, and may be used for the production of adsorbents
145 [59,60], catalyst support [61,62], fertilizers [63] or soil amender [64]. Therefore, the
146 bio-oil and the gases were the volatiles fed into the reforming step together with the
147 steam required.

148 **Table 2.** Yields of biomass pyrolysis products (wt %) at 500 ºC.

Compound	Yield (wt %)
Gas	**7.33**
CO	3.38
CO_2	3.27
Hydrocarbons (C_1-C_4)	0.68
Bio-oil	**75.33**
Acids	2.73
Aldehydes	1.93
Alcohols	2.00
Ketones	6.37
Phenols	16.49
Furans	3.32
Saccharides	4.46
Water	25.36
Char	**17.34**

149

150 The reforming step has been carried out under the following operating conditions: 600
151 ºC; space time, 20 g_{cat} min $g_{volatiles}^{-1}$; S/B ratio, 4. It should be noted that, using this
152 space time, operation is under kinetic regime and the deactivation is fast, which eases
153 the comparison of the deactivation in successive reaction-regeneration cycles. In order
154 to obtain a suitable fluidization of the bed, 25 g of a mixture of catalyst and sand has
155 been used, with their particle sizes ranging being 0.4-0.8 mm and 0.30-0.35 mm,
156 respectively. These experimental conditions were selected according to the results
157 obtained in previous studies dealing with the analysis of the influence of operating
158 conditions [5,20]. Once conversion decreased considerably, the reaction was stopped
159 and a sample of the deactivated catalyst was taken for analysis.

160 After each reaction step, coke combustion has been performed in situ in the reforming
161 reactor, with temperature and air concentration ramp being as follows: i) 600 ºC for 90

min, with air (in N_2) concentration increasing every 15 min from 10 to 100 vol % in order to avoid hot spots causing Ni sintering, and; ii) temperature increasing from 600 to 700 ºC in 60 min, and maintained this temperature for another 60 min. As coke was being removed, the concentration of CO_2 has been monitored at the reactor outlet, and a sample of the catalyst has been taken after the coke combustion step.

Once the combustion of coke has been finished, the catalyst has been reduced again at 710 ºC with a stream of 10 vol % of H_2 in N_2. At this point, another sample of the reduced catalyst has been analyzed. This process was repeated for six consecutive reforming-regeneration cycles.

2.4. Reaction indices

The process results have been quantified according to the following reaction indices: conversion, yields of C containing compounds, and H_2 yield and production. The reforming conversion has been calculated as the ratio between the C units in the gaseous product stream (F_{gas}) and those contained in the pyrolysis volatiles fed into the reforming step ($F_{volatiles}$), without considering the C contained in the char, which was continuously removed from the CSBR.

$$X(\%) = \frac{F_{gas}}{F_{volatiles}} 100 \quad (1)$$

The yield of each C containing compound in the product stream of the reforming step has been calculated based on the volatiles derived from biomass pyrolysis:

$$Y_i(\%) = \frac{F_i}{F_{volatiles}} 100 \quad (2)$$

where F_i is the molar flow rate of C in each product i.

H_2 yield is given as a percentage of the maximum allowable by stoichiometry:

$$Y_{H_2}(\%) = \frac{F_{H_2}}{F^0_{H_2}} 100 \quad (3)$$

where F_{H2} and F_{H2}^0 are the actual molar flow rate of H_2 and the maximum corresponding to stoichiometry (following eq. (4)), respectively.

$$C_nH_mO_k + (2n-k)H_2O \rightarrow nCO_2 + (2n+m/2-k)H_2 \quad (4)$$

H_2 production has been defined by mass unit of the biomass in the feed:

$$P_{H_2}(wt\ \%) = \frac{m_{H_2}}{m_0}100 \quad (5)$$

where m_{H2} is the mass flow rate of the H_2 produced and m_0 is the mass flow rate of the biomass fed into the CSBR, respectively.

3. Results

3.1. Recovery of catalyst activity

In order to explain the product distribution obtained in the reforming step, the following reactions have been considered: steam reforming of oxygenated compounds (eq. (6)), CH_4 (eq. (7)) and C_2-C_4 hydrocarbons (eq. (8)), water gas shift (WGS) reaction (eq. (9)) and cracking of oxygenated compounds (eq. (10)).

$$C_nH_mO_k + (n-k)H_2O \rightarrow nCO + (n+m/2-k)H_2 \quad (6)$$

$$CH_4 + H_2O \rightarrow CO + 3H_2 \quad (7)$$

$$C_rH_s + rH_2O \rightarrow rCO + (r+s/2)H_2 \quad (8)$$

$$CO + H_2O \leftrightarrow CO_2 + H_2 \quad (9)$$

$$C_nH_mO_k \rightarrow C_xH_yO_z + C_aH_b + CH_4 + CO + CO_2 + C \quad (10)$$

First, the product distribution obtained at zero time on stream in different reforming-regeneration cycles has been analyzed. Figure 1 displays the conversion (graph a) and yields of H_2 (graph b), CO_2 (graph c), CO (graph d), CH_4 (graph e), C_2-C_4 hydrocarbons (graph f) and non-reacted oxygenates (graph g), at zero time on stream for the successive reaction-regeneration steps. As observed, the catalyst recovers only partially its reforming activity after the regeneration step. Although initial conversion is almost

full in the first and second cycles, it decreases slightly from the second to the fifth cycle, obtaining a value of 90.1 % in the last cycle (Figure 1a). It should be pointed out that the irreversible loss of catalyst activity attenuates progressively and is negligible in the fifth and sixth cycles. The cause of this irreversible deactivation is the sintering of Ni crystallites (as proven afterwards), whose effect on product distribution at zero time on stream is similar to that aforementioned for conversion.

As observed, H_2 and CO_2 yields decrease from 93.5 to 72.4 % (Figure 1b) and from 88.6 to 69.5 % (Figure 1c), respectively, from the first to the sixth cycle, with a progressively less pronounced trend in subsequent reaction-regeneration cycles. Consequently, H_2 production (eq (5)) decreases from 11.2 to 7.8 % from the first to the sixth cycle. On the other hand, CO, CH_4 and C_2-C_4 hydrocarbon yields (Figures 1d, 1e and 1f, respectively) increase with reforming-regeneration cycles, from 10.6 to 17.5 %, 0.6 to 2.6 % and 0 to 0.6 %, respectively. This increase in by-product yields as catalyst deactivation progresses is due to the attenuation in the reaction rates of CH_4 and C_2-C_4 hydrocarbon reforming and CO conversion by WGS reaction. Moreover, the yield of non-converted oxygenates (Figure 1g) also increases from 0.3 to 9.9 %, whose decomposition reactions also contribute to the formation of by-products enhanced by catalyst deactivation [65-68]. It is noteworthy that the difference in the results is progressively smaller as more successive reaction-regeneration cycles are carried out, with this difference being insignificant when the results for the fifth and sixth reactions are compared.

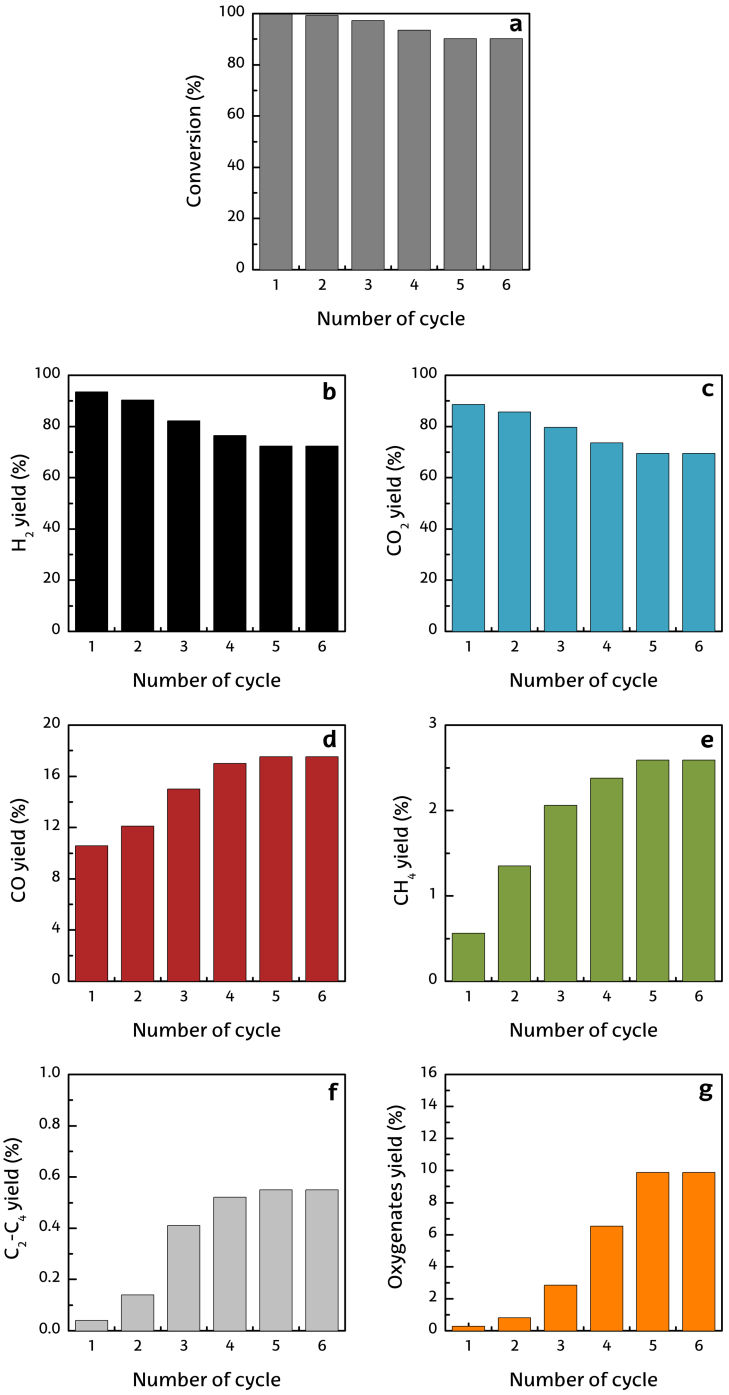

Figure 1. Values at zero time on stream for the conversion (a) and yields of H_2 (b), CO_2 (c), CO (d), CH_4 (e), C_2-C_4 hydrocarbons (f), and non-converted oxygenates (g) for six consecutive reaction-regeneration cycles.

In order to evaluate the effect irreversible deactivation has on catalyst deactivation, the evolution with time on stream of conversion and products yields throughout consecutive reaction-regeneration cycles is shown in Figure 2. It should be noted that the total duration of the cycle has a significant decreasing trend until the 3rd cycle, which is

238 explained by the decay in catalyst activity as the number of cycles is increased.
239 Nevertheless, subsequent to the 3rd cycle the total duration is maintained at around 40
240 min on stream. As observed, the conversion (Figure 2a) and the yields of H_2, CO_2 and
241 CO (Figures 2b) decrease with time on stream due to the catalyst deactivation for
242 reforming and WGS reactions. Moreover, following the trend mentioned above for the
243 deterioration of catalyst activity (Figure 1), the decrease in the initial cycles is faster as
244 the number of cycles is increased, and similar in the last cycles. This trend is
245 characteristic of deactivation mechanisms by coke deposition, which is enhanced by the
246 following causes: i) sintering of Ni crystallites, which favor coke deposition [69,70],
247 and; ii) the higher concentration of oxygenates in the reaction medium, in particular the
248 phenolic compounds derived from the pyrolysis of biomass lignin, which are the main
249 coke precursors [71,72]. Furthermore, the yield of on-converted oxygenates increases
250 with time on stream, as observed in Figure 2b, due to the attenuation of oxygenate
251 reforming and WGS reaction.

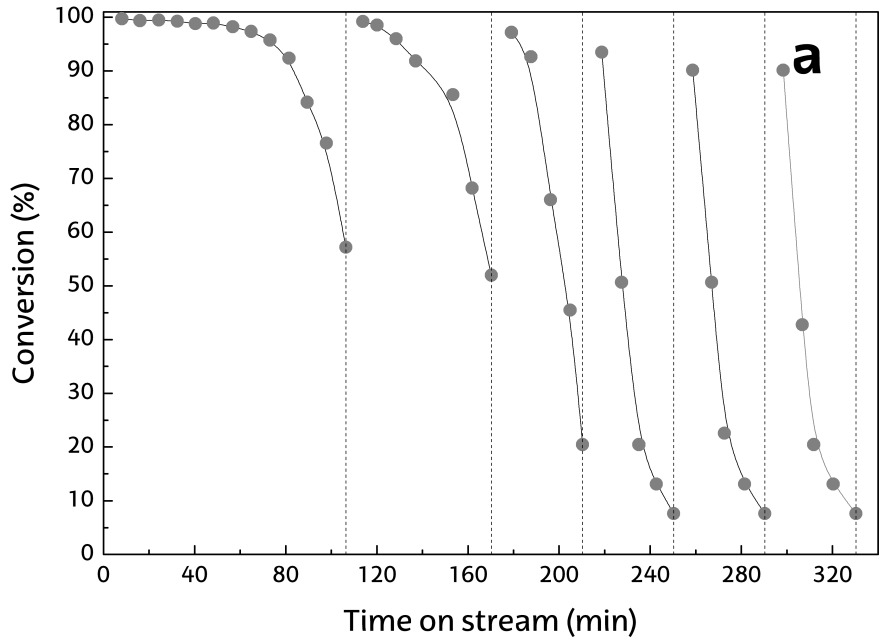

252

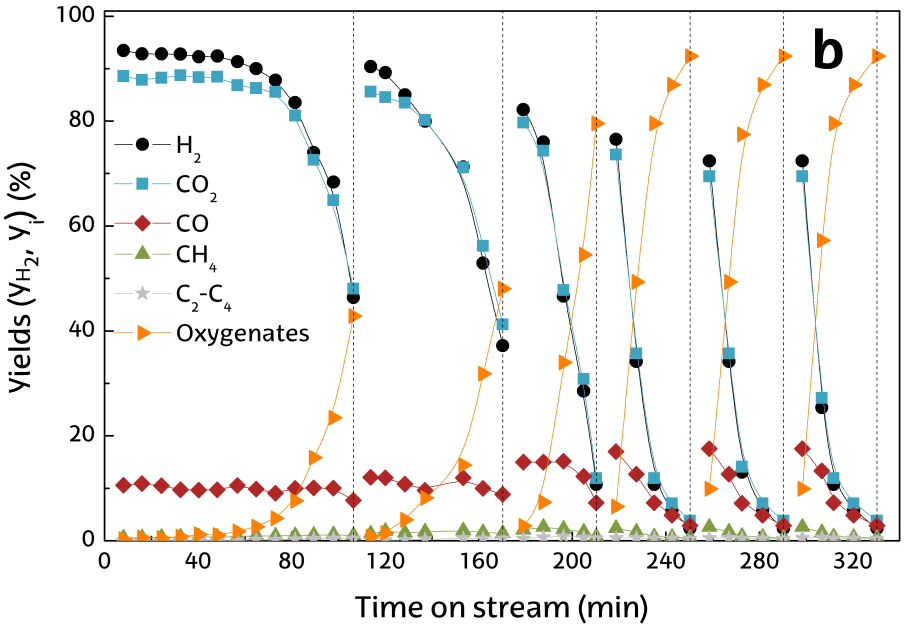

253

254 **Figure 2.** Evolution of conversion (a) and product yields (b) with time on stream for 6
255 consecutive reaction-regeneration cycles.

256 Figure 3 shows the evolution of gaseous product composition with time on stream. The
257 concentration of H_2 at zero time on stream decreases as the number of reaction-
258 regeneration cycles is increased, whereas the concentration of CO, CH_4 and C_2-C_4

hydrocarbons increases, given that catalyst activity for reforming and WGS reactions decreases due to Ni sintering. Moreover, the rate of decrease in H_2 concentration and the rate of increase in CO, CH_4 and C_2-C_4 concentrations with time on stream in each cycle is higher as the number of cycles is increased. These results are qualitatively similar to those obtained in the literature in the reforming of bio-oil [73-75].

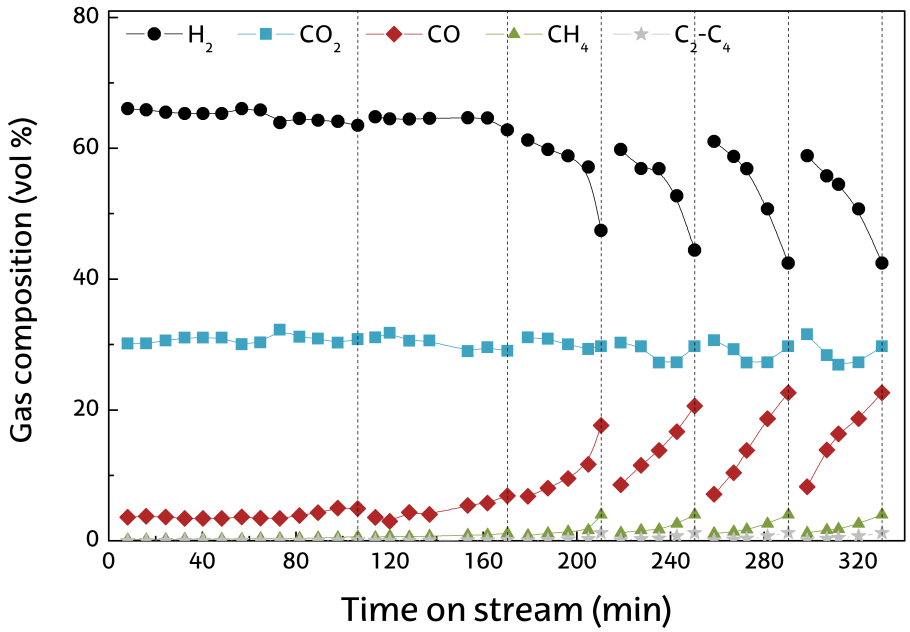

Figure 3. Evolution of the gaseous product composition with time on stream for 6 consecutive reforming-regeneration cycles.

3.2. Deactivated catalyst characterization

The fast catalyst deactivation in each reaction step is attributable to coke deposition. Consequently, the deactivated catalysts have been analyzed by TPO in order to study the content and nature of the coke deposited. Moreover, the TEM analysis has allowed determining the type of coke and the evolution of Ni crystallites size.

The TPO profiles for the catalysts deactivated after each reaction cycle have been plotted in Figure 4. The TPO profile of the catalyst deactivated in the first reaction shows two well-differentiated peaks, with their maxima being at 430 ºC and 560 ºC. Based on the literature about the analysis of the coke formed in the reforming of bio-oil and pure oxygenates, these peaks correspond to the combustion of two coke fractions: i)

277 an amorphous coke (coke I) encapsulating Ni metallic sites, which burns at low
278 temperatures and, and; ii) a more structured coke (coke II) detached from Ni metallic
279 sites, which burns at higher temperatures. It should also be pointed out that the
280 structured coke increases with time on stream, given that it presumably comes from the
281 evolution of encapsulating coke towards more graphitized structures. Thus, the high
282 peak obtained for coke II in the first cycle is mainly attributable to the high duration of
283 the reaction (106 min), whereas in the second cycle this peak is significantly lower due
284 to the lower duration (64 min) of the reaction. From the third to the sixth cycle, the
285 duration of the reactions is short (around 40 min in all the reactions), and so the
286 structured coke is not evolved and the deposited coke is exclusively amorphous. Table 3
287 shows the coke content in the deactivated catalyst for different reforming-regeneration
288 cycles and, as observed, coke content is mainly related to the duration of each reaction.
289 It should be pointed out that coke content is similar from the third to the sixth cycle.

290 The TEM images of the deactivated catalysts (Figure 5) show the presence of non-
291 structured coke, but no carbon filaments are observed. This absence of carbon filaments
292 is characteristic of the coke deposited in the reforming of bio-oil [68,76], as opposed to
293 the reforming of CH_4 and hydrocarbons and volatiles from plastic pyrolysis, in which
294 the presence of structured coke is considerable [25,36,43,77].

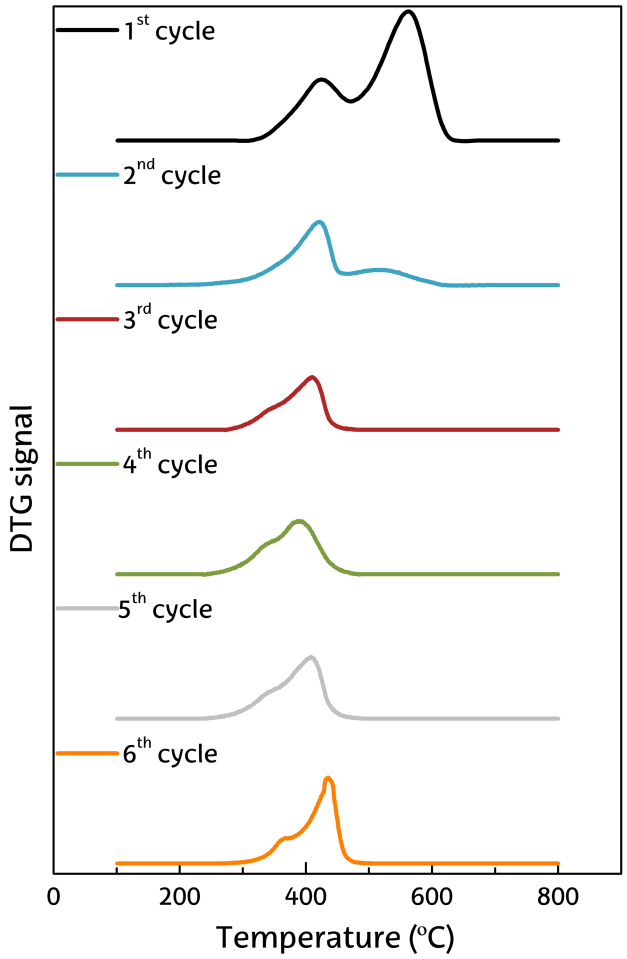

295

296 **Figure 4.** TPO profiles of the catalysts deactivated for 6 consecutive reaction-
297 regeneration cycles.

298 **Table 3.** Coke content (wt %) of the catalysts deactivated for 6 consecutive
299 reforming- regeneration cycles.

Cycle	C_C, wt %
1	9.9
2	3.8
3	2.3
4	3.0
5	2.9
6	2.9

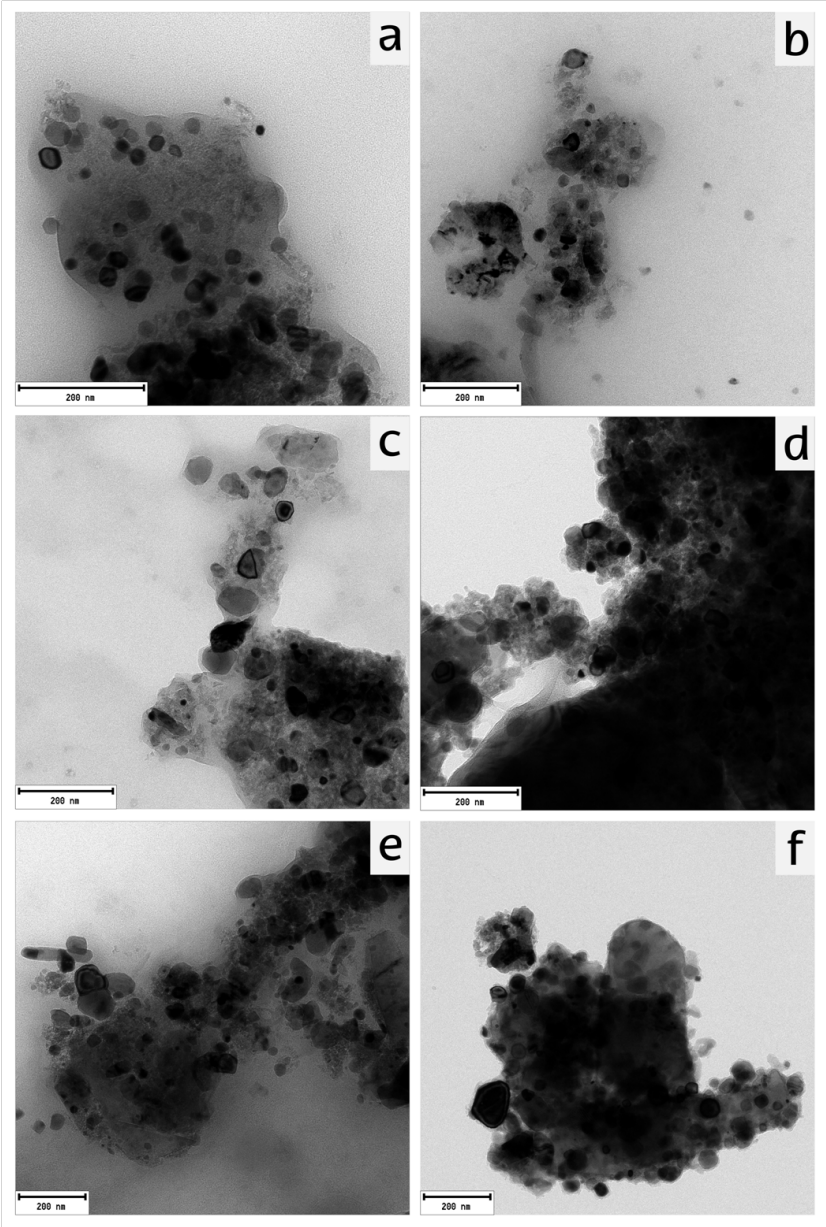

Figure 5. TEM images of the catalysts deactivated in successive reaction-regeneration cycles, corresponding to the 1st (a), 2nd (b), 3rd (c), 4th (d), 5th (e) and 6th (f) reactions.

3.3. Regenerated catalyst characterization

The sintering of Ni sites is presumably the cause of irreversible deactivation in successive reaction-regeneration cycles. The TEM images in Figure 5 reveal an increase in Ni crystallite size in the deactivated catalysts. This increase has been quantified by X-ray diffraction (XRD) analysis of the catalysts regenerated in successive reaction-

regeneration cycles. Table 4 shows the Ni crystallite sizes calculated applying the equation by Debye-Scherrer. As observed, the size increases considerably as the number of reforming-regeneration cycles is higher, which is evidence of Ni sintering. Nevertheless, the reaction temperature (600 ºC) is barely above the Tamman temperature, [78] and therefore Ni sintering probably occurs during the reduction (prior to the reforming reaction) and regeneration steps carried out at 700 ºC. Table 4 also shows that the increase in the average Ni crystallite size is progressively lower as more successive reaction-regeneration cycles are conducted, with the trend being a value of 55 nm after the fourth and fifth cycles. This result is in line with the trend of irreversible deactivation (Figure 2), which attenuates progressively as the number of successive reaction-regeneration cycles is increased.

Table 4. Evolution of average Ni crystallite size for 6 consecutive reaction-regeneration cycles.

Cycle	Crystallite size, nm
Fresh	25
1	40
2	48
3	50
4	55
5	55

The regenerated catalysts have also been characterized by temperature programmed reduction (TPR). The TPR profiles in Figure 6 correspond to the fresh catalyst, and those regenerated after the first, third and fifth cycles. The fresh catalyst shows a very wide main peak, with the maximum being at around 450-470 ºC, attributed to the reduction of NiO species with different interaction degree with α-Al_2O_3 support, and another peak at 680 ºC, which corresponds to the reduction of $NiAl_2O_4$ spinel [79,80]. It is evident that the reducibility of Ni species is lower once the coke has been burnt in the first cycle. Moreover, a lower temperature is required to reduce these species as the number of cycles is increased. This trend is explained by the lower dispersion of Ni

particles due to the higher Ni crystallite size, thereby decreasing the intensity of the metal-support interaction and easing its reduction [81]. Furthermore, it is also observed that the peak corresponding to the $NiAl_2O_4$ spinel has almost disappeared in the first regeneration step, which is evidence that the regeneration temperature is not enough for the reconstruction of the spinel (reaction of NiO species with α-Al_2O_3 support).

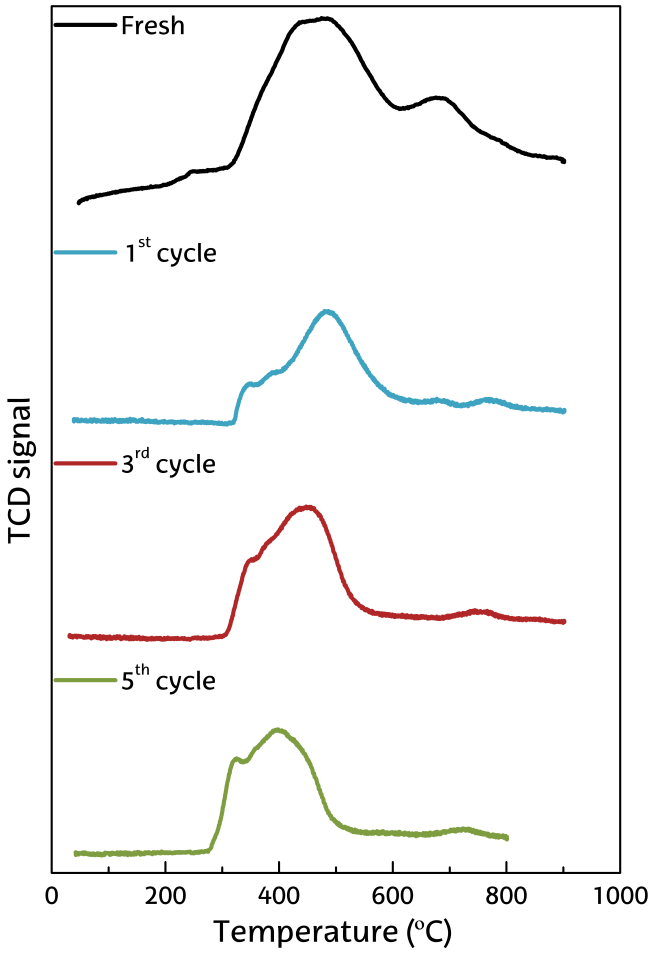

Figure 6. TPR profiles for the fresh catalyst and catalysts regenerated in consecutive reaction-regeneration cycles.

The aforementioned results concerning the analyses of the catalysts deactivated and regenerated in successive reaction-regeneration cycles allow establishing that Ni sintering is the cause of irreversible deactivation, presumably during the regeneration step carried out by coke combustion at a maximum temperature of 700 ºC. Zhao and Lu [50] carried out ethanol reforming and they also reported that Ni species are sintered in

346 the regeneration step due to the heat produced in the combustion of the coke, leading to
347 a sudden increase in catalyst surface. This irreversible deactivation is a drawback for
348 use of this catalyst in industry. Nevertheless, the results obtained in this work have
349 proven that Ni sintering progressively attenuates in the successive cycles and the
350 catalyst reaches a stable structure with reproducible results after the fourth regeneration
351 step. Different strategies for attenuating Ni sintering may also be suitable as an
352 alternative for catalyst stabilization, such as coke combustion at lower temperature. Ni
353 sintering also attenuates with a previous equilibration step of the catalyst consisting in a
354 high temperature treatment in order to increase the presence of Ni in the $NiAl_2O_4$ spinel
355 phase. However, these treatments do not guarantee the reproducibility of the results in
356 reaction-regeneration cycles, or they may cause a decrease in catalyst activity.

357 **4. Conclusions**

358 The commercial catalyst used in the reforming of biomass pyrolysis volatiles is active
359 and selective for H_2 production. However, consecutive reaction-regeneration cycles
360 show that it is only partially regenerated by coke combustion. Thus, conversion and H_2
361 yield at zero time on stream decrease from the first to the sixth cycle, from 99.7 to 90.1
362 % and from 93.5 to 72.4 %, respectively. Due to this irreversible deactivation, the
363 deactivation in each reaction step is faster as the number of successive cycles is
364 increased.

365 The analysis of deactivated and regenerated catalysts allows establishing that sintering
366 of Ni species is the cause of irreversible deactivation, which presumably occurs in the
367 regeneration step. Ni crystallite size increases as the number of reforming-regeneration
368 cycles is higher, thereby decreasing dispersion and catalyst activity for reforming and
369 WGS reactions. The increase in Ni crystallite size leads to the formation of exclusively
370 amorphous coke, without the presence of filamentous carbon.

371 Consequently, the results obtained throughout six consecutive reforming-regeneration
372 cycles reveal catalyst activity decay occurs presumably in the regeneration step
373 (performed at 700 ºC). Nevertheless, the phenomenon of Ni sintering attenuates in
374 successive regeneration steps, in which the catalyst reaches a pseudo-stable state.
375 Accordingly, conversion and product yields attain a stable evolution with time on

stream (reproducible results) beyond the fourth cycle, which is a relevant fact for use of this catalyst in industry.

Acknowledgement

This work has been carried out with the financial support from the Ministry of Economy and Competitiveness of the Spanish Government (CTQ2016-75535-R (AEI/FEDER, UE) and CTQ-2015-69436-R (MINECO/FEDER, UE)) and the Basque Government (IT748-13). Aitor Arregi and Itsaso Barbarias thank the University of the Basque Country for their postgraduate grants (UPV/EHU 2017 and 2016, respectively).

References

[1] W. Nabgan, T.A. Tuan Abdullah, R. Mat, B. Nabgan, Y. Gambo, M. Ibrahim, A. Ahmad, A.A. Jalil, S. Triwahyono, I. Saeh, Renewable Sustainable Energy Rev. 79 (2017) 347-357.

[2] J. Fermoso, F. Rubiera, D. Chen, Energy Environ. Sci. 5 (2012) 6358-6367.

[3] R. Parajuli, T. Dalgaard, U. Jørgensen, A.P.S. Adamsen, M.T. Knudsen, M. Birkved, M. Gylling, J.K. Schjørring, Renewable Sustainable Energy Rev. 43 (2015) 244-263.

[4] L. Wang, D. Li, M. Koike, S. Koso, Y. Nakagawa, Y. Xu, K. Tomishige, Appl Catal A 392 (2011) 248-255.

[5] A. Arregi, G. Lopez, M. Amutio, I. Barbarias, J. Bilbao, M. Olazar, RSC Adv. 6 (2016) 25975-25985.

[6] F. Chen, C. Wu, L. Dong, A. Vassallo, P.T. Williams, J. Huang, Appl. Catal. B 183 (2016) 168-175.

[7] L. Dong, C. Wu, H. Ling, J. Shi, P.T. Williams, J. Huang, Fuel 188 (2017) 610-620.

[8] X. Zhao, J. Ren, J. Cao, F. Wei, C. Zhu, X. Fan, Y. Zhao, X. Wei, Energy Fuels 31 (2017) 4054-4060.

[9] P. Iovane, A. Donatelli, A. Molino, Biomass Bioenergy 56 (2013) 423-431.

[10] A. Erkiaga, G. Lopez, M. Amutio, J. Bilbao, M. Olazar, Fuel Process. Technol. 116 (2013) 292-299.

[11] T. Ogi, M. Nakanishi, Y. Fukuda, K. Matsumoto, Fuel 104 (2013) 28-35.

[12] A. Di Carlo, D. Borello, M. Sisinni, E. Savuto, P. Venturini, E. Bocci, K. Kuramoto, Int. J. Hydrogen Energy 40 (2015) 9088-9095.

[13] L. Garcia, R. French, S. Czernik, E. Chornet, Appl Catal A 201 (2000) 225-239.

[14] Z. Wang, Y. Pan, T. Dong, X. Zhu, T. Kan, L. Yuan, Y. Torimoto, M. Sadakata, Q. Li, Appl Catal A 320 (2007) 24-34.

[15] A. Remiro, B. Valle, A.T. Aguayo, J. Bilbao, A.G. Gayubo, Energy Fuels 27 (2013) 7549-7559.

[16] F. Seyedeyn-Azad, J. Abedi, S. Sampouri, Ind. Eng. Chem. Res. 53 (2014) 17937-17944.

[17] H. Xie, Q. Yu, Z. Zuo, Z. Han, X. Yao, Q. Qin, Int. J. Hydrogen Energy 41 (2016) 2345-2353.

[18] F. Bimbela, J. Ábrego, R. Puerta, L. García, J. Arauzo, Appl. Catal. B 209 (2017) 346-357.

[19] A. Arregi, M. Amutio, G. Lopez, J. Bilbao, M. Olazar, Energy Convers. Manage. 165 (2018) 696-719.

[20] A. Arregi, G. Lopez, M. Amutio, M. Artetxe, I. Barbarias, J. Bilbao, M. Olazar, Fuel 216 (2018) 233-244.

[21] L. Santamaria, G. Lopez, A. Arregi, M. Amutio, M. Artetxe, J. Bilbao, M. Olazar, Appl. Catal. B 229 (2018) 105-113.

[22] I. Barbarias, G. Lopez, J. Alvarez, M. Artetxe, A. Arregi, J. Bilbao, M. Olazar, Chem. Eng. J. 296 (2016) 191-198.

426 [23] I. Barbarias, G. Lopez, M. Artetxe, A. Arregi, L. Santamaria, J. Bilbao, M. Olazar,
427 J. Anal. Appl. Pyrolysis 122 (2016) 502-510.

428 [24] I. Barbarias, G. Lopez, M. Amutio, M. Artetxe, J. Alvarez, A. Arregi, J. Bilbao, M.
429 Olazar, Appl. Catal. A 527 (2016) 152-160.

430 [25] I. Barbarias, G. Lopez, M. Artetxe, A. Arregi, J. Bilbao, M. Olazar, Energy
431 Convers. Manage. 156 (2018) 575-584.

432 [26] A. Arregi, M. Amutio, G. Lopez, M. Artetxe, J. Alvarez, J. Bilbao, M. Olazar,
433 Energy Convers. Manage. 136 (2017) 192-201.

434 [27] C. Rioche, S. Kulkarni, F.C. Meunier, J.P. Breen, R. Burch, Appl. Catal. B 61
435 (2005) 130-139.

436 [28] Y. Park, T. Namioka, S. Sakamoto, T. Min, S. Roh, K. Yoshikawa, Fuel Process.
437 Technol. 91 (2010) 951-957.

438 [29] A.C. Basagiannis, X.E. Verykios, Int. J. Hydrogen Energy 32 (2007) 3343-3355.

439 [30] T. Namioka, A. Saito, Y. Inoue, Y. Park, T. Min, S. Roh, K. Yoshikawa, Appl.
440 Energy 88 (2011) 2019-2026.

441 [31] M. Koike, C. Ishikawa, D. Li, L. Wang, Y. Nakagawa, K. Tomishige, Fuel 103
442 (2013) 122-129.

443 [32] C. Wu, L. Dong, J. Onwudili, P.T. Williams, J. Huang, ACS Sustainable Chem.
444 Eng. 1 (2013) 1083-1091.

445 [33] X. Xiao, J. Cao, X. Meng, D.D. Le, L. Li, Y. Ogawa, K. Sato, T. Takarada, Fuel
446 103 (2013) 135-140.

447 [34] A. Donatelli, P. Iovane, A. Molino, Fuel 89 (2010) 2721-2728.

448 [35] S. Luo, Y. Zhou, C. Yi, Energy 44 (2012) 391-395.

449 [36] J.C. Acomb, C. Wu, P.T. Williams, Appl. Catal. B 147 (2014) 571-584.

450 [37] J. Chen, J. Sun, Y. Wang, Ind. Eng. Chem. Res. 56 (2017) 4627-4637.

451 [38] A. Ochoa, I. Barbarias, M. Artetxe, A.G. Gayubo, M. Olazar, J. Bilbao, P. Castaño,
452 Appl. Catal. B 209 (2017) 554-565.

453 [39] M. Marquevich, S. Czernik, E. Chornet, D. Montané, Energy Fuels 13 (1999)
454 1160-1166.

455 [40] C.E. Efika, C. Wu, P.T. Williams, J. Anal. Appl. Pyrolysis. 95 (2012) 87-94.

456 [41] M.A. Nahil, X. Wang, C. Wu, H. Yang, H. Chen, P.T. Williams, RSC Adv. 3
457 (2013) 5583-5590.

458 [42] Q.M.K. Waheed, P.T. Williams, Energy Fuels 27 (2013) 6695-6704.

459 [43] C. Wu, P.T. Williams, Appl. Catal. B 96 (2010) 198-207.

460 [44] Z. Abdelsadek, M. Sehailia, D. Halliche, V.M. Gonzalez-Delacruz, J.P. Holgado,
461 K. Bachari, A. Caballero, O. Cherifi, J. CO_2 Util. 14 (2016) 98-105.

462 [45] B. Rego de Vasconcelos, D. Pham Minh, P. Sharrock, A. Nzihou, Catal. Today
463 (2017), https://doi.org/10.1016/j.cattod.2017.05.092

464 [46] E.B. Pereira, N. Homs, S. Martí, J.L.G. Fierro, P. Ramírez de la Piscina, J. Catal.
465 257 (2008) 206-214.

466 [47] L. Bednarczuk, P. Ramírez de la Piscina, N. Homs, Int. J. Hydrogen Energy 40
467 (2015) 5256-5263.

468 [48] L. Bednarczuk, P. Ramírez de la Piscina, N. Homs, Int. J. Hydrogen Energy 41
469 (2016) 19509-19517.

470 [49] C. Montero, A. Remiro, A. Arandia, P.L. Benito, J. Bilbao, A.G. Gayubo, Fuel
471 Process. Technol. 152 (2016) 215-222.

472 [50] X. Zhao, G. Lu, Int. J. Hydrogen Energy 41 (2016) 13993-14002.

[51] L. Oar-Arteta, A.T. Aguayo, A. Remiro, J. Bilbao, A.G. Gayubo, Ind. Eng. Chem. Res. 54 (2015) 11285-11294.

[52] L. Oar-Arteta, A. Remiro, J. Vicente, A.T. Aguayo, J. Bilbao, A.G. Gayubo, Fuel Process. Technol. 126 (2014) 145-154.

[53] E.A. Sanchez, R.A. Comelli, Int. J. Hydrogen Energy 37 (2012) 14740-14746.

[54] L.F. Bobadilla, A. Penkova, A. Álvarez, M.I. Domínguez, F. Romero-Sarria, M.A. Centeno, J.A. Odriozola, Appl. Catal. A 492 (2015) 38-47.

[55] D. Li, M. Koike, L. Wang, Y. Nakagawa, Y. Xu, K. Tomishige, ChemSusChem 7 (2014) 510-522.

[56] G. Lopez, M. Olazar, M. Amutio, R. Aguado, J. Bilbao, Energy Fuels 23 (2009) 5423-5431.

[57] M. Amutio, G. Lopez, R. Aguado, J. Bilbao, M. Olazar, Energy Fuels 26 (2012) 1353-1362.

[58] M. Amutio, G. Lopez, M. Artetxe, G. Elordi, M. Olazar, J. Bilbao, Resour. Conserv. Recycling. 59 (2012) 23-31.

[59] J. Alvarez, G. Lopez, M. Amutio, J. Bilbao, M. Olazar, Bioresour. Technol. 170 (2014) 132-137.

[60] H. Bamdad, K. Hawboldt, S. MacQuarrie, Renewable Sustainable Energy Rev. 81 (2018) 1705-1720.

[61] P. Lu, Q. Huang, Y. Chi, J. Yan, J. Anal. Appl. Pyrolysis 127 (2017) 47-56.

[62] M. Hu, M. Laghari, B. Cui, B. Xiao, B. Zhang, D. Guo, Energy 145 (2018) 228-237.

[63] M. Uchimiya, S. Hiradate, M.J. Antal, ACS Sustainable Chem. Eng. 3 (2015) 1642-1649.

497 [64] C.R. Smith, E.M. Buzan, J.W. Lee, ACS Sustainable Chem. Eng. 1 (2013) 118-
498 126.

499 [65] S. Czernik, R. French, C. Feik, E. Chornet, Ind. Eng. Chem. Res. 41 (2002) 4209-
500 4215.

501 [66] J.A. Medrano, M. Oliva, J. Ruiz, L. García, J. Arauzo, Energy 36 (2011) 2215-
502 2224.

503 [67] S. Liu, M. Chen, L. Chu, Z. Yang, C. Zhu, J. Wang, M. Chen, Int. J. Hydrogen
504 Energy 38 (2013) 3948-3955.

505 [68] A. Remiro, B. Valle, A.T. Aguayo, J. Bilbao, A.G. Gayubo, Fuel Process. Technol.
506 115 (2013) 222-232.

507 [69] D. Chen, K.O. Christensen, E. Ochoa-Fernández, Z. Yu, B. Tøtdal, N. Latorre, A.
508 Monzón, A. Holmen, J. Catal. 229 (2005) 82-96.

509 [70] K.O. Christensen, D. Chen, R. Lødeng, A. Holmen, Appl. Catal. A 314 (2006) 9-
510 22.

511 [71] B. Valle, B. Aramburu, M. Olazar, J. Bilbao, A.G. Gayubo, Fuel 216 (2018) 463-
512 474.

513 [72] B. Valle, B. Aramburu, P.L. Benito, J. Bilbao, A.G. Gayubo, Fuel 216 (2018) 445-
514 455.

515 [73] S. Czernik, R. Evans, R. French, Catal. Today 129 (2007) 265-268.

516 [74] B. Valle, A. Remiro, A.T. Aguayo, J. Bilbao, A.G. Gayubo, Int. J. Hydrogen
517 Energy 38 (2013) 1307-1318.

518 [75] J. Remón, F. Broust, G. Volle, L. García, J. Arauzo, Int. J. Hydrogen Energy 40
519 (2015) 5593-5608.

520 [76] A. Ochoa, B. Aramburu, M. Ibáñez, B. Valle, J. Bilbao, A.G. Gayubo, P. Castaño,
521 ChemSusChem 7 (2014) 2597-2608.

[77] I. Barbarias, M. Artetxe, G. Lopez, A. Arregi, J. Bilbao, M. Olazar, Fuel Process. Technol. 171 (2018) 100-109.

[78] J.A. Moulijn, A.E. van Diepen, F. Kapteijn, in: Anonymous Handbook of Heterogeneous Catalysis, Wiley-VCH Verlag GmbH & Co. KGaA, 2008.

[79] J.M. Rynkowski, T. Paryjczak, M. Lenik, Appl. Catal. A 106 (1993) 73-82.

[80] J.G. Seo, M.H. Youn, S. Park, I.K. Song, Int. J. Hydrogen Energy 33 (2008) 7427-7434.

[81] R.M. Navarro, R. Guil-Lopez, A.A. Ismail, S.A. Al-Sayari, J.L.G. Fierro, Catal. Today 242 (2015) 60-70.